V International Conference on Simulation for Additive Manufacturing
Sim-AM 2025
F. Auricchio, M. Carraturo and S. Morganti (Eds)

NUMERICAL ANALYSIS OF GYROID STRUCTURE PERFORMANCES IN HEAT SINK ENVIRONMENT

BELLI N.*, GAUDENZI G.† AND GIORLEO L.†

*Advance Prototyping Laboratory,
Mechanical and Industrial Departement,
University of Brescia, Via Branze 38, Italy
e-mail: nicole.belli@unibs.it, web page: https://sites.google.com/unibs.it/lpa

Key words: Additive Manufacturing, CFD, Gyroid, Simulation, TPMS

1 INTRODUCTION

Heat sinks are thermal management components integrated into electronic devices, designed to maintain operating temperatures below critical thresholds to ensure reliability and functional integrity [1]. At the same time, the trend towards miniaturization of electronic components has led to a significant increase in power density per unit volume. This increase in power density results in higher operating temperatures, which can potentially cause overheating and compromise the reliability of the device [2].

For this reason, new geometries are required to enhance the heat dissipation of these electronic devices. A solution made possible only by modern manufacturing technologies, such as Additive Manufacturing (AM), is the use of Triply Periodic Minimal Surface (TPMS) structures. TPMS structures are characterized by a high surface-to-volume ratio, low weight, and remarkable mechanical properties [3]. In addition to their mechanical properties, TPMS structures also offer advantages in terms of heat dissipation. Among the various TPMS types, the Primitive, Gyroid, I-WP, and Diamond structures have been most extensively studied in the field of heat exchangers. The Diamond structure appears to be the most effective due to its superior convective heat transfer capabilities [4, 5]. Nonetheless, the study of the Gyroid structure remains of interest because of its good heat transfer performance combined with the low pressure drop it introduces to the fluid [6].

In literature most analyses on the cooling efficiency of TPMS structures focus on simulations in simple straight channels. Therefore, in this study a modular demonstrator that closely approximates a realistic scenario (non-uniform power source, and complex heat sink design) in the field of liquid-cooled heat sinks ([7]) was considered. The aim of this research is investigating the performances of TPMS structures in heat exchange by numerical simulation. Seven different structures were designed varying the TPMS geometrical features (extension in width, length, and thickness). These decisions involve potential constraints related to the demonstrator assembly and fluid connections. Moreover, the design and simulation should comply with the requirements for minimizing maximum temperatures, ensuring uniformity of the average temperature, and maintaining low pressure drops.

2 MATERIALS AND METHODS

The research aims at understanding how different geometries affect thermal exchange in a cooler implemented with TPMS structures. The heat sink components were designed by Computer-Aided Design (CAD), and Computational Fluid Dynamics (CFD) simulations were performed to evaluate the efficiency in cooling down the heat sink, heated by a power source. The software tools and

platforms used to design the geometry are listed in the 2.1 Section. The methodologies adopted in the design and simulation steps are explained in detail in the 2.2 Section.

2.1 MATERIALS

The geometries were developed using Rhino 3D, SolidWorks, and nTopology. In detail, Rhino 3D and SolidWorks were used for modeling and managing the overall cooler geometries, and nTopology to generate the TPMS structure geometries. CFD simulations were performed using FloEFD, integrated in the Simcenter 3D environment.

2.2 METHODS

The research composes of two main steps: the design and the simulation. Since the aim of this study is to evaluate the influence of different TPMS geometries on heat exchange in a cooler, the demonstrator was designed with interchangeable inserts (Section 2.2.1). Subsequently, to investigate the influence of the extension and thickness of the structure, seven TPMS structures were generated from the same unit cell (size $10 \times 10 \times 10$ mm^3), (Section 2.2.2). To evaluate and compare the structures efficiency in heat exchange, CFD simulations were performed. Briefly, the top surface of the device is heated by power sources, and a cooling liquid enters the circuit at a set temperature and cools down the heated surface. Materials, boundary conditions, and goals are defined in Section 2.2.3. Before performing the actual simulations a mesh analysis was carried out in Section 2.2.3.

2.2.1 DEMONSTRATOR DESIGN

The modular demonstrator closely approximates a realistic scenario in the field of liquid-cooled heat sinks, complying with design constraints. In particular, the device external dimensions ($336\text{mm}\times 180\text{mm}\times 44\text{mm}$) are comparable to those of power electronics devices available on the market [7] (see Figure 1a). The demonstrator composes of base, cover, TPMS inserts, input and output connectors, and armored resistors.

The base contains a U-shaped liquid circuit (rectangular cross section 10 mm x 66 mm), Figure 1. The cover is a block with a maximum thickness of 21 mm in the circuit region and minimum thickness 16 mm in the outer part. Six housing regions are present on the cover for the TPMS inserts positioning. Each TPMS insert is composed of two parts a support (see Figure 1c for dimensions) and the TPMS structure see Section 2.2.2. Inlet and outlet connectors are located on the same face (as shown in Figure 1b), similarly to real power electronics devices. 18 armored resistors, designed starting from real 25 W resistors geometries [8] are positioned on the cover surface, as shown in Figure 1d. In summary, resistors are assumed perfectly attached to the cover, TPMS inserts are positioned by interference between the cover and the base, and the cover is assumed attached to the base.

The position of the device in the CAD design space is defined by the origin point (O) (visible in Figure 1b), whose coordinates are given in Equation 1.

$$x_O = 86.20\text{mm}; \qquad y_O = -2.14\text{mm}; \qquad z_O = 93.53\text{mm} \tag{1}$$

2.2.2 TPMS STRUCTURES DESIGN

TPMS inserts, as previously mentioned, are composed of two parts (support and TPMS structure). This section focuses on the TPMS structure design. The Gyroid structure was modeled using nTopol-

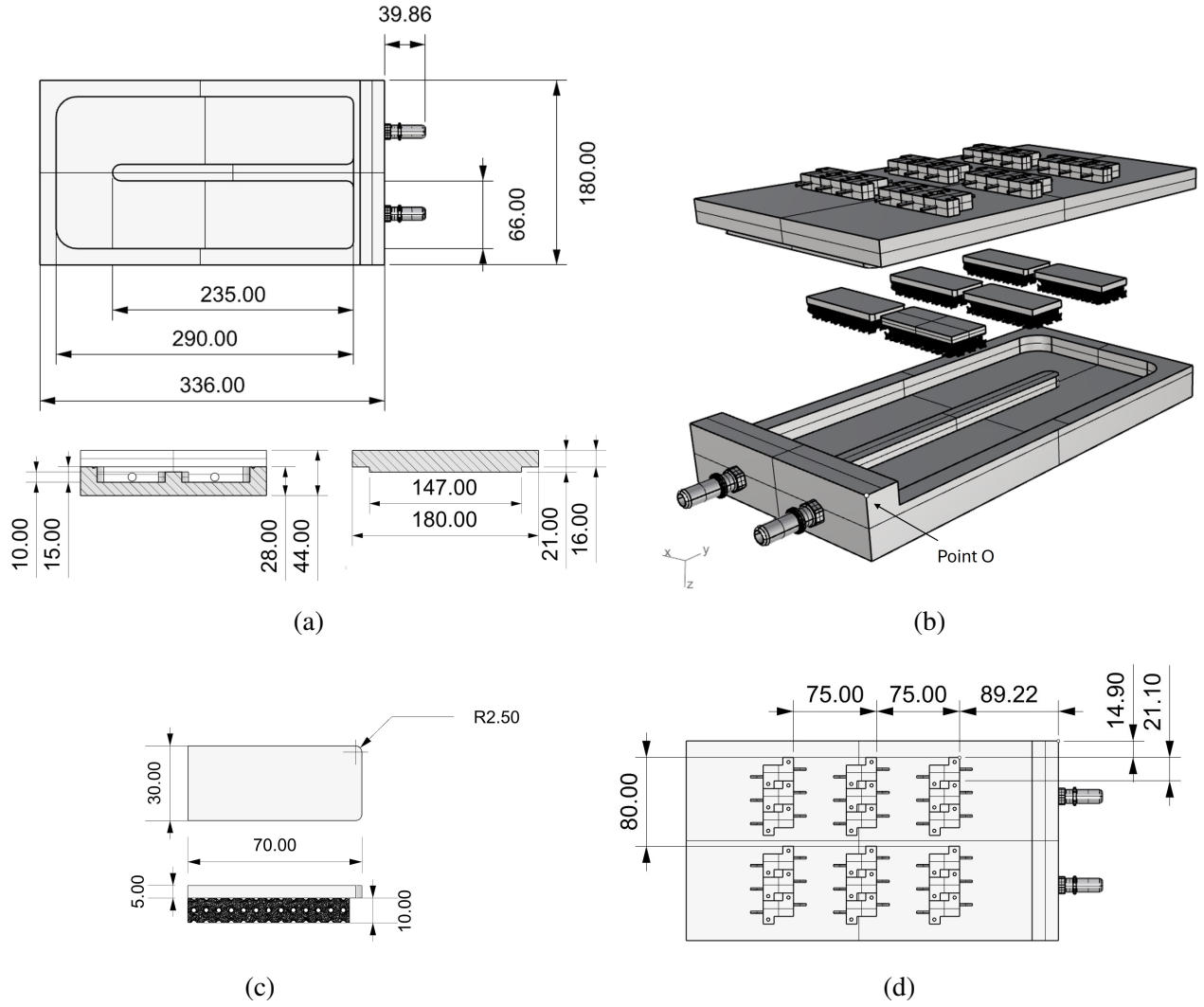

Figure 1: Liquid cooling demonstrator geometry. (a) Dimensioned drawing of the demonstrator; (b) Exploded CAD view showing the internal components; (c) Dimensioned drawing of the single TPMS insert; (d) Top view of the demonstrator with resistors, and their dimensions.

ogy software, starting from a unit cell measuring $10\ \mathrm{mm} \times 10\ \mathrm{mm} \times 10\ \mathrm{mm}$ with a wall thickness of $1\ \mathrm{mm}$ (Table 1-(a)). Starting from the unit cell, the TPMS structures were derived, considering different configurations. Three kind of scenarios were simulated to investigate the effect of Gyroid structures features as width, length, and thickness, in Table 1.

In every scenario the structure height is equal to the height of the channel and of the unit cell ($10\ \mathrm{mm}$).

To carry out the analysis, the TPMS width extension was varied to investigate its effect on the flow path and heat exchange. Two kinds of insert were then designed, occupying respectively the 68.2% and the 100% of the channel width. One composes of three TPMS structures growing from the support and each structure is located exactly under a resistor. The dimensions of each structure are $30\mathrm{mm} \times 15\mathrm{mm}$ (see Table 1-(b)). The second one consists of a single TPMS structure that extends along the entire channel width, its dimensions are $30\ \mathrm{mm} \times 66\ \mathrm{mm}$ (Table 1-(c)).

The second analysis, aimed at evaluating the influence of length, was carried out considering three

TPMS structures with different longitudinal length. In particular, starting from the $30\text{mm} \times 66\text{mm}$ structure two additional inserts were designed by changing the length of 50%, in both negative and positive directions (see Table 1-(c) and 1-(d)). The results are two structures with lengths of 15mm and 45mm respectively.

Finally, to asses the influence of the structure thickness, this feature was varied. Starting from the $30\text{mm} \times 66\text{mm}$ structure four thicknesses were considered 0.5mm, 1.0mm, 1.5mm, and 2.5mm, as shown in Table 1-(f), 1-(c), 1-(g), and 1-(h).

2.2.3 CFD SETUP AND MESH SENSITIVITY ANALYSIS

Simulations were performed to assess if and how different inserts would help in thermal dissipation in a liquid cooled heat sink in steady state conditions. Briefly, the top surface of the device is heated and the cooling liquid enters from the inlet connector at a set temperature of $23\ ^{\circ}C$ to keep the temperature as low as possible. In this section, the setup of the thermo-fluid dynamic simulations is presented. Materials (Table 2), boundary conditions, and goals must be defined. In a heat exchange study materials are pivotal: aluminum is a good and common choice for a cooler because of its thermal conductivity. Different kinds of aluminum were chosen: the AlSi10Mg for the inserts (suited for components feasible only by AM, such as TPMS), and Al5083 H32 for base and cover. The cooling liquid consists of a mixture $50\% - 50\%$ of H_2O and glycol.

The boundary conditions applied to the faces of the domain are all of the slip type, while the gravitational acceleration vector has only a z-component of $9.81\ \text{m/s}^2$. For the boundary conditions on the solid surfaces, a no-slip condition is applied. For the cooling fluid subdomain, two boundary conditions are imposed. A flow with a volumetric flow rate of $8\ \text{l/min}$ is imposed at the inlet, with the outlet set to ambient pressure $101325\ \text{Pa}$. The 18 surface power sources, a total power of $400\ W$ is evenly divided among the resistors and applied on the bottom surface of the resistors, in contact with the cover. The external domain dimensions are $800 \times 800 \times 800\ \text{mm}^3$.

The temperature (T_{avg} and T_{max}) and pressure (ΔP) values were collected for all the seven structures designed visible in Table 1-(b):(h), and for the empty demonstrator scenario. The results were compared in three steps accordingly to the three analysis carried out. In detail, the demonstrator without the TPMS structures (empty demonstrator) was compared to the ones with the 30_15_1 and 30_66_1. Then the 30_66_1 insert was compared to the structures with plus or minus 50% in length (15_66_1, 45_66_1). Finally the 30_66_1 insert was compared to the others with different thickness ($30\_66\_0.5$, 30_66_1, $30\_66\_1.5$, and $30\_66\_2.5$). In all scenarios the colored map for temperatures and flow velocity were considered and compared (in the results, for conciseness reasons, only two representative scenarios are shown in Figure 4).

To precisely assess and compare the thermal efficiency of the different structures temperature is evaluated in 18 points are defined on the cover near the heating elements. In detail, the points are arranged according to the coordinates in Table 3 (note that the z coordinate is the same for all and is equal to $93.53\ \text{mm}$ as they rest on the same plane) as illustrated in Figure 2. The average temperature (T_{avg}) of the lid is defined as the arithmetic mean of the individual temperature values (Equation 2), while the maximum temperature (T_{max}) is the highest of the 18 values acquired (Equation 3).

$$T_{avg} = \frac{\sum_{i=1}^{18} T_i}{18} \tag{2}$$

$$T_{max} = max(T_i) \qquad 1 \leq i \leq 18 \tag{3}$$

$$\Delta P = P_{in} - P_{out} \tag{4}$$

Moreover, the pressure drop (ΔP) between inlet and outlet (Equation 4) and the dimensionless Reynolds (Re) and Nusselt (Nu) numbers were also considered (Equations 5 and 6).

Table 1: Unit cell and TPMS structures dimensions and graphical display.

Label	**Lenght** [mm]	**Width** [mm]	**Thickness** [mm]	**Figure**
Unit cell	10	10	1	 (a)
30_15_1	30	15	1	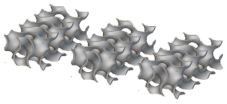 (b)
30_66_1	30	66	1	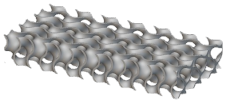 (c)
15_66_1	15	66	1	 (d)
45_66_1	45	66	1	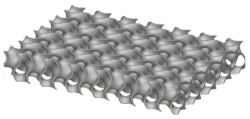 (e)
30_66_0.5	30	66	0.5	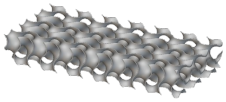 (f)
30_66_1.5	30	66	1.5	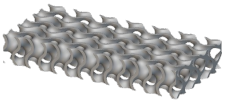 (g)
30_66_2.5	30	66	2.5	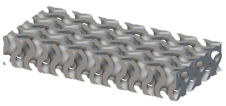 (h)

Table 2: List of the materials used in the simulation and their features, where I/O is for input/output.

	Material	**Thermal Conductivity** $[W/m \cdot K]$	**Density** $[kg/m^3]$
Base	Al5083 H32	117	2600
Cover	Al5083 H32	117	2600
Armored resistances	Aluminum	237	2689
I/O connectors	Brass	71	8400
TPMS structures	AlSi10Mg	165	2670
Cooling Liquid	$50\% - 50\%$ $H_2O -$ glycol	0.54	1076 ± 3

Table 3: x and y coordinates for the 18 temperature measurement points at $z = 93.53$ mm.

Point number	**x** [mm]	**y** [mm]	**Point number**	**x** [mm]	**y** [mm]
1	104, 79	100.72	**10**	205.79	250.72
2	125.79	100.72	**11**	226.79	250.72
3	146.79	100.72	**12**	247.79	250.72
4	104, 79	175.72	**13**	205.79	175.72
5	125.79	175.72	**14**	226.79	175.72
6	146.79	175.72	**15**	247.79	175.72
7	104, 79	250.72	**16**	205.79	100.72
8	125.79	250.72	**17**	226.79	100.72
9	146.79	250.72	**18**	247.79	100.72

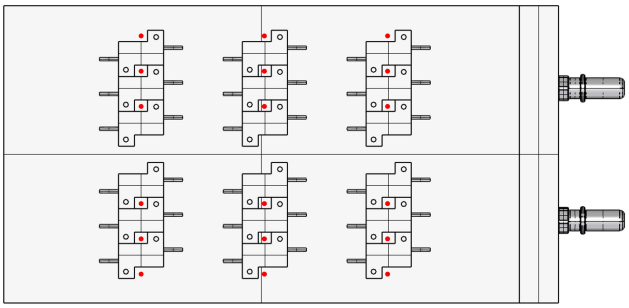

Figure 2: Top view of the demonstrator with the 18 acquisition point in red.

The Re and Nu numbers are dimensionless parameters, they characterize fluid behavior and thermal performance of the structure, respectively. In detail, the Re number describes the degree of turbulence in the fluid flow. The Nu number, defined as the ratio between convective and conductive heat transfer, is an indicator of the thermal performance of the TPMS structure in this study.

The dimensionless numbers are calculated locally at the volume of the TPMS structures (Re_{LOCj} and Nu_{LOCj}) and then arithmetically averaged on the entire circuit (Re and Nu).

$$Re_{LOCj} = \frac{\rho \cdot v_j \cdot D_h}{\mu} \qquad Re = \frac{\sum_{j=1}^{n} Re_{LOCj}}{n} \tag{5}$$

$$Nu_{LOCj} = \frac{HTC_l \cdot D_h}{k_f} \qquad HTC_j = \frac{Q_{tot}}{A_{wall} \cdot (T_{wall} - T_{fluid})} \qquad Nu = \frac{\sum_{j=1}^{n} Nu_{LOCj}}{n} \tag{6}$$

where ρ is the fluid density, v_j is the average velocity in the fluid volume region of the TPMS structures, D_h is the hydraulic diameter calculated as $D_h = \frac{4 \cdot V_f}{A_{wall}}$, μ_l is the dynamic viscosity of the fluid, k_f is the thermal conductivity of the fluid. Moreover, Q_{tot} is the heat exchanged by convection, A_{wall} is the heat transfer surface area of the TPMS structure, and $(T_{wall} - T_{fluid})$ is the temperature difference between the surface of the TPMS structure and the fluid. n in the number of the TPMS structure in the different configurations.

An overall comparison was carried out among the seven inserts considered during the study. T_{avg}, T_{max}, ΔP, Re, and Nu were considered. Five classes were defined for each parameter considered. The range of each class is calculated as the difference between the maximum (Max_{value}) and minimum (Min_{value}) values of the parameter considered divided by the number of classes (5).

As an example, if a parameter minimum value is 27 and the range (difference between its maximum and minimum values divided by 5) is 0.2 the first class is defined in the range between 27.0 and 27.2, the second class is between 27.2 and 27.4, and so on up to the fifth class.

Given one insert, according to the class the parameter value belongs to a grade from 1 to 5 is attributed; lower the numerical value of the grade better the performance. T_{avg}, T_{max}, and ΔP should be minimized to obtain better performances. Therefore, a grade of 1 is attributed if the parameter belongs to the first class, a grade of 2 if it belongs to the second class, and so on up to a grade of 5 if the value belongs to the fifth class. Conversely, Re, and Nu number should be high to have a better insert performance. Then, a grade of 5 is given if the parameter belongs to the first class, 4 if it is in the second class, towards 1 if the value is in the fifth class.

The last setting necessary to start a simulation is the mesh. A mesh sensitivity analysis was carried out on the empty demonstrator. To avoid errors due to spatial discretizations, a mesh convergence study was first carried out, by analyzing the temperature values at control points reported in Table 3 on the cover and the T_{avg} and T_{max} and the ΔP as the mesh refinement level varied (coarse, rough, medium, and fine).

The Ratio Factor (RF) was set at 4 and four levels of mesh refinement were obtained; RF determines the rate at which the mesh cell size increases from the boundary toward the interior of the domain. Meanwhile the global level of the mesh is 3 for the coarse mesh, 4 for the rough one, 5 for the medium one, and 6 for the fine one.

Finally, the medium mesh (refinement level 5) was chosen for the simulations. Indeed, the fine mesh requires really long times compared to the medium one and and the difference in temperature and pressure drop is acceptable.

Table 4: Mesh sensitivity analysis performed on the empty circuit. The table reports the number of mesh elements and the corresponding CPU time required for each simulation case.

	Total cells	**Fluid cells**	**Solid cells**	**Fluid-solids cells**	**Solver CPU time** [s]
Coarse	1.33×10^5	7.20×10^4	6.11×10^4	3.02×10^4	17
Rough	2.40×10^5	1.30×10^5	1.09×10^5	5.34×10^4	298
Medium	3.94×10^5	2.35×10^5	1.59×10^5	7.86×10^4	614
Fine	2.10×10^6	1.55×10^6	5.50×10^5	3.10×10^5	3857

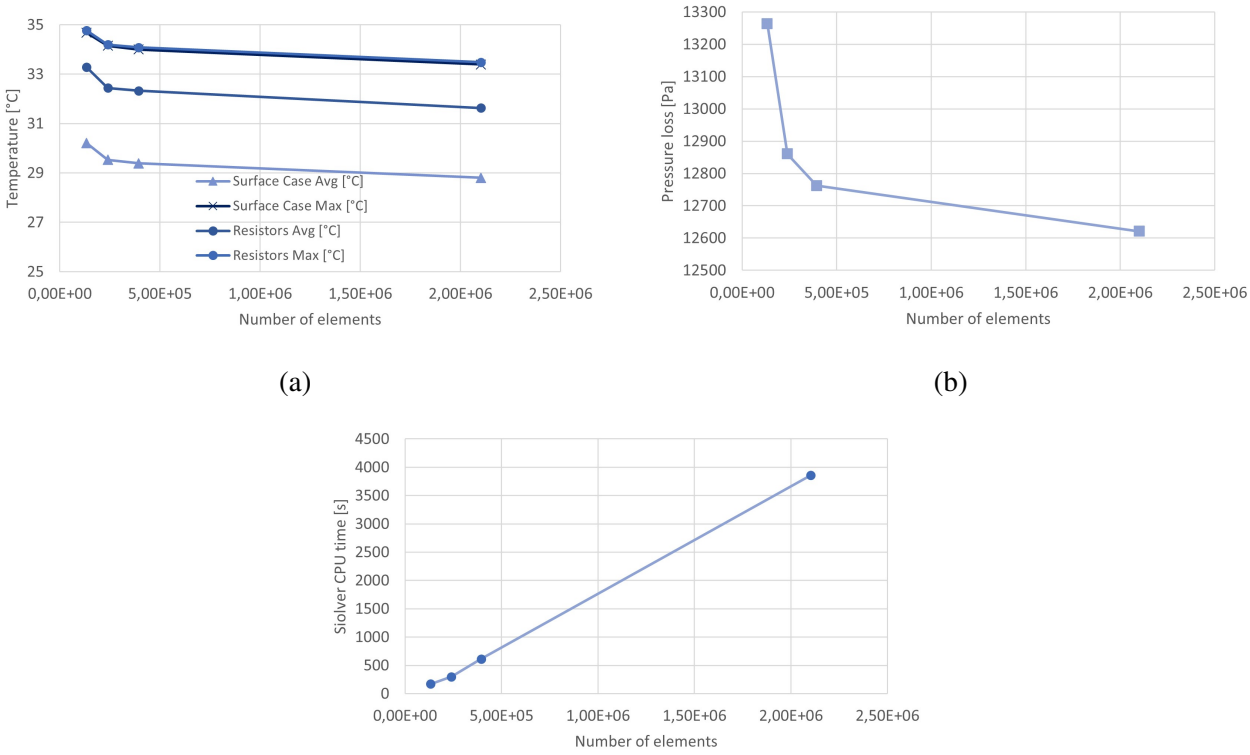

(a) (b)

(c)

Figure 3: Average temperature (a), pressure drop (b), and solver CPU Time (c) as function of the number of Mesh elements of the empty circuit configuration. The investigation was carried out for coarse, rough, medium, and fine mesh, see table.

3 RESULTS AND DISCUSSION

The first analysis, aimed at assessing the effect of transverse extension of the TPMS structure (empty demonstrator, 30_15_1 structure, and 30_66_1 structure), showed the highest cover temperatures in the empty demonstrator due to the absence of material under the resistive elements (see Figure 4d, 4e, and 4f). The flow distribution observed in the velocity plot (Figure 4a) is asymmetric. This behavior is attributed to the off-centered position of the inlet channel, which generates higher pressure on the outer side. The 30_15_1 structure configuration exhibits a higher inlet pressure compared to the empty case, due to the presence of the TPMS structures. The interaction of the fluid with the first

set of TPMS elements generates inlet vortexes and backflow, which results in a pressure increase in the initial section of the channel. The Nu and Re numbers are the highest for the 30_66_1 (Table 6), and the maximum velocity is witnessed inside its voids. As both Nu and Re numbers increase the convective heat transfer over the conductive one raises and the regime within the TPMS volume becomes more turbulent. The results show that as Nu and Re numbers increase the T_{avg} decreases, while the ΔP increases (Tables 5 and 6). These observations indicate that, among the considered ones, the most effective configuration in reducing cover temperatures is the 30_66_1.

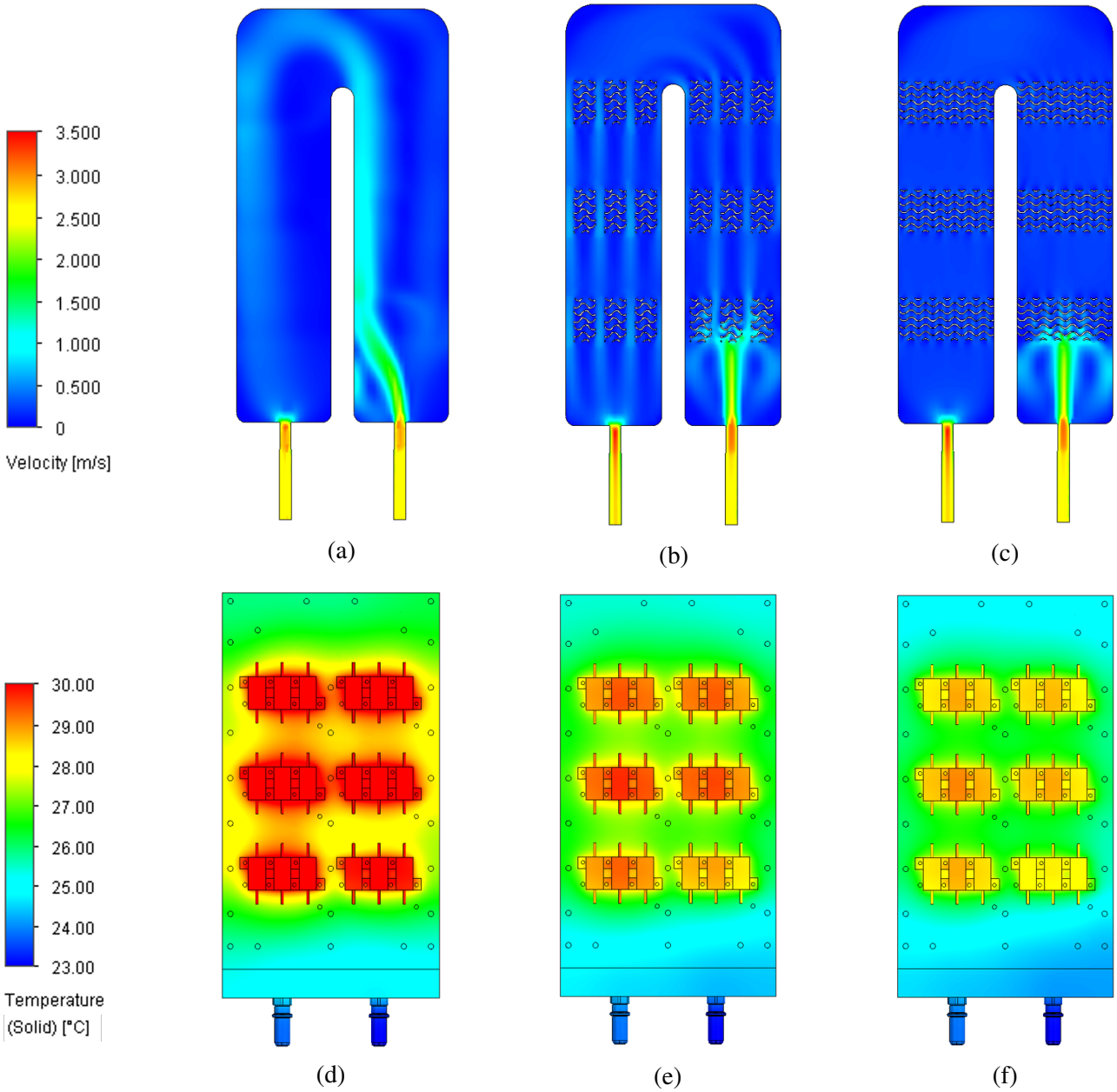

Figure 4: Cut plot of velocity obtained at half the channel height, for the empty channel (a), the 30_15_1 (b), and 30_66_1 (c); Surface plot of temperature on the top surface of the demonstrator for the empty channel (d), the 30_15_1 (e), and 30_66_1 (f).

The values of ΔP and T_{avg} on the cover for the second class of simulations (aiming at assessing the TPMS structure length influence) are collected in Table 5. Table 6 shows the Nu and Re numbers; extended structures (45_66_1) are less efficient in terms of dissipation and turbulence generation than shorter ones (15_66_1). The reduction in the longitudinal extension of the TPMS resulted in a decrease in ΔP of approximately 7%, but led to an increase in T_{avg} of about 3%. Conversely, for the extended TPMS the ΔP increased by approximately 4%, while the reduction in T_{avg} did not exceed 2% compared to the reference case (reference length 30 mm). A non-linear decrease in cover temperature was observed with increasing longitudinal extension of the TPMS. Heat dissipation proved to be more effective when the TPMS was positioned directly beneath the heat source, and optimal performance was achieved when the TPMS structure dimensions were maintained at $10\text{mm} \times 30\text{mm} \times 66\text{mm}$.

The third analysis focused on the structure 30_66_1, varying the wall thickness within a range between 0.5 mm and 2.5mm. Increasing the TPMS thickness in this configuration resulted in lower cover temperatures, as shown in Table 5, but also led to higher ΔP. The Re number, reported in Table 6, decreases when increasing the thickness from 0.5mm to 1.5 mm, but rises again at 2.5mm due to the increased fluid velocity in the voids of the structure. This increase in velocity has a stronger effect on turbulence generation than the reduction in hydraulic diameter. The Nu number decreases with increasing thickness.

The overall comparison among the results obtained for all the seven inserts was carried out by grading the structure performances for all the parameters investigated, as detailed in the 2.2 section. In Table 7 the extension of the classes for each parameter are calculated. The ranking of all the TPMS inserts is presented in Table 8, here all the grades given to the structures for each parameter are listed. As previously mentioned, lower the grade better the performance of the structure for that specific parameter. There is no structure that has the best performance for all the parameters (all grades 1). Moreover, in some cases ($30\_66\_2.5$; 15_66_1) when the performance is optimal for a certain feature (grade 1), it is the worst for another characteristics (grade 5). Summarizing, there is not an actual optimum. Overall the structure 30_66_1 can be considered the best compromise: its final $\sum$ grade (8) is the lowest.

Table 5: Resulting T_{avg}, $St.Dev._{Tavg}$, T_{max} and ΔP values for all the configurations investigated.

	$\mathbf{T_{avg}}$ $[°C]$	$\mathbf{St.Dev._{Tavg}}$	$\mathbf{T_{max}}$ $[°C]$	$\mathbf{\Delta P}$ $[Pa]$
30_15_1	28.31	0.61	29.08	13726
30_66_1	27.72	0.55	28.41	14664
15_66_1	28.65	0.64	29.48	13670
45_66_1	27.25	0.53	27.88	15283
30_66_0.5	28.06	0.58	28.79	14128
30_66_1.5	27.53	0.55	28.21	15222
30_66_2.5	27.19	0.55	27.85	19263

Table 6: Resulting Re and Nu numbers values for all the configurations investigated.

	Re	**Nu**
30_15_1	344	28.13
30_66_1	514	31.74
15_66_1	530	35.26
45_66_1	492	30.55
30_66_0.5	537	34.60
30_66_1.5	490	29.95
30_66_2.5	497	24.26

Table 7: Definition of five classes by defining the range extension as the span over the number of classes (5), where the span is obtained subtracting the parameter minimum value (Min_{value}) from the maximum one (Max_{value}). Maximum and minimum values are selected comparing the results in Table 5 and 6.

	$\mathbf{T_{avg}}$ $[°C]$	$\mathbf{T_{max}}$ $[°C]$	$\mathbf{\Delta P}$ $[Pa]$	**Re**	**Nu**
$\mathbf{Max_{value}}$	28.65	29.48	19263	537	35.26
$\mathbf{Min_{value}}$	27.19	27.85	13670	344	24.26
Span	1.46	1.63	5592	193	11.01
Range	0.29	0.33	1118	39	2.20

Table 8: Ranking of the configurations investigated. The value of each parameter can belong to one of five classes. A grade from 1 to 5 is given to the configuration according to the class it belongs, as explained in 3. Lower the grade better the performance.

	grade_$\mathbf{T_{avg}}$	**grade_$\mathbf{T_{max}}$**	**grade_$\mathbf{\Delta P}$**	**grade_Re**	**grade_Nu**	$\sum$**grades**
30_66_1	2	2	1	1	2	**8**
45_66_1	1	1	2	2	3	**9**
30_66_0.5	3	3	1	1	1	**9**
30_66_1.5	2	2	2	2	3	**11**
15_66_1	5	5	1	1	1	**13**
30_66_2.5	1	1	5	2	5	**14**
30_15_1	4	4	1	5	4	**18**

4 CONCLUSIONS

The effect of the geometrical features of TPMS structures was investigated by changing extension in width, length and thickness. The study assessed that dimensions are crucial in determining TPMS performances. Depending on the aim some features should be prioritized in the design of a heat sink.

- Average and maximum temperatures decrease with the TPMS wall thickness.
- Pressure drop decrease as the TPMS structure extension in the longitudinal direction reduces.
- Turbulence increases as the TPMS wall thickness decreases.
- Convective heat exchange improves by shortening the longitudinal extension of the TPMS structure.

The simulations demonstrate that there is not an actual optimum. The best compromise between minimizing pressure drop and maximizing cooling efficiency is achieved with the TPMS insert 30_66_1, that has width equal to the circuit channel and a wall thickness of $1.0\ \mathrm{mm}$.

REFERENCES

[1] Abbas, E. F., (2024) AN OVERVIEW OF HEAT SINK TECHNOLOGY, International Journal of Applied Mechanics and Engineering, vol. 29 (4), 1-23. https://doi.org/10.59441/ijame/192127.

[2] Haldun M. Ozaktas, Hakan Oksuzoglu, R. F.W. Pease, Joseph W. Goodman, (1992) Effect on scaling of heat removal requirements in three-dimensional systems, International Journal of Electronic, vol. 73 (6), 1227-1232. https://doi.org/10.1080/00207219208925792.

[3] F. Torri, F. Berni, S. Fontanesi, S. Mantovani, M. Giacalone, S. Defanti, E. Bassoli, G. Colombini, (2023) Evaluation of TPMS Structures for the Design of High Performance Heat Exchangers, SAE Technical Papers. https://doi.org/10.4271/2023-24-0125.

[4] Dutkowski, K.; Kruzel, M.; Rokosz, K., (2022) Review of the State-of-the-Art Uses of Minimal Surfaces in Heat Transfer, Energies, vol. 15 (21), 7994. https://doi.org/10.3390/en15217994.

[5] W. Tang, H. Zhou, Y. Zeng, M. Yan, C. Jiang, P. Yang, Q. Li, Z. Li, J. Fu, Y. Huang, Y. Zhao, (2023) Analysis on the convective heat transfer process and performance evaluation of Triply Periodic Minimal Surface (TPMS) based on Diamond, Gyroid and Iwp, International Journal of Heat and Mass Transfer, vol. 201 (6), 1227-1232. https://doi.org/10.1016/j.ijheatmasstransfer.2022.123642.

[6] Liu, J., Cheng, D., Oo, K., Pan, W., McCrimmon, T.-L., & Bai, S. (2024) Optimization of Triply Periodic Minimal Surface Heat Exchanger to Achieve Compactness, High Efficiency, and Low-Pressure Drop. Energies, 17(20), 5141. https://doi.org/10.3390/en17205141

[7] (2025) https://www.cobogroup.net/prodotti/inverter/.

[8] (2022) https://it.rs-online.com/web/p/resistenze-corazzate/2522726.